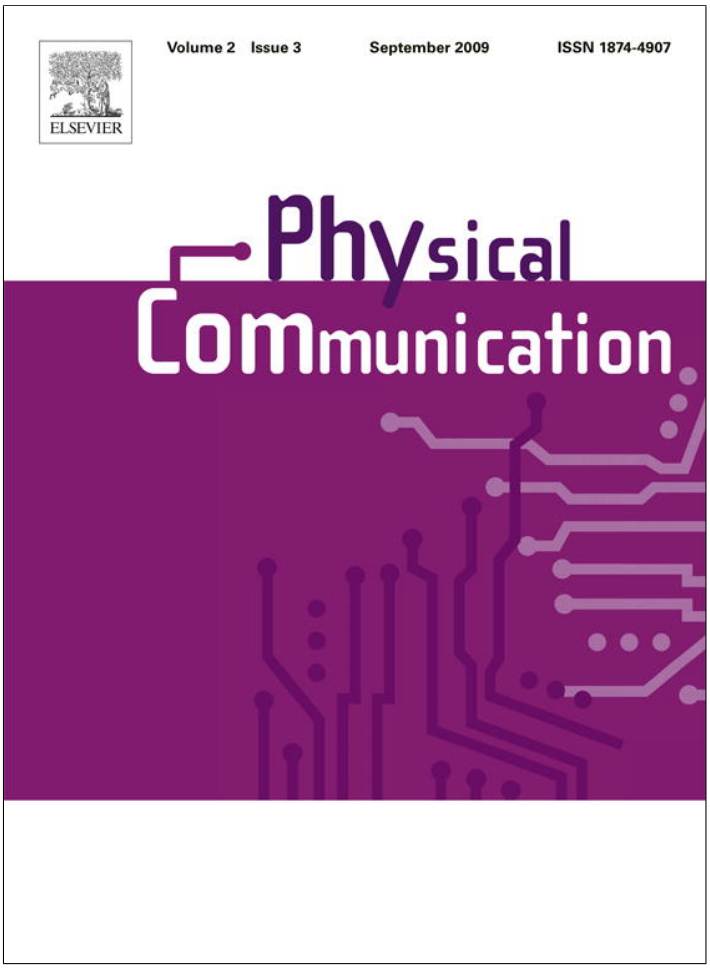

Physical Communication 2 (2009) 167–183

Contents lists available at ScienceDirect

Physical Communication

journal homepage: www.elsevier.com/locate/phycom

Full length article

Signal propagation techniques for wireless underground communication networks

Ian F. Akyildiz [a,*], Zhi Sun [a], Mehmet C. Vuran [b]

[a] Broadband Wireless Networking Laboratory, School of Electrical & Computer Engineering, Georgia Institute of Technology, Atlanta, GA, 30332, United States

[b] Department of Computer Science and Engineering, University of Nebraska-Lincoln, Lincoln, NE 68588, United States

ARTICLE INFO

Keywords:
Wireless networks
Channel model
Soil medium
Underground mine
Tunnel
Magnetic induction
Waveguide

ABSTRACT

Wireless Underground Communication Networks (WUCNs) consist of wireless devices that operate below the ground surface. These devices are either (i) buried completely under dense soil, or (ii) placed within a bounded open underground space, such as underground mines and road/subway tunnels. The main difference between WUCNs and the terrestrial wireless communication networks is the communication medium. In this paper, signal propagation characteristics are described in these constrained areas. First, a channel model is described for electromagnetic (EM) waves in soil medium. This model characterizes not only the propagation of EM waves, but also other effects such as multipath, soil composition, water content, and burial depth. Second, the magnetic induction (MI) techniques are analyzed for communication through soil. Based on the channel model, the MI waveguide technique for communication is developed to address the high attenuation challenges of MI waves through soil. Furthermore, a channel model, i.e., the *multimode model*, is provided to characterize the wireless channel for WUCNs in underground mines and road/subway tunnels. The multimode model can characterize two cases for underground communication, i.e., the *tunnel* channel and the *room-and-pillar* channel. Finally, research challenges for the design communication protocols for WUCNs in both underground environments are discussed based on the analysis of the signal propagation.

1. Introduction

Wireless Underground Communication Networks (WUCNs) constitute one of the promising application areas of the recently developed wireless networking techniques. The WUCNs consist of wireless devices that operate below the ground surface. These devices are either (i) buried completely under dense soil or (ii) placed within a bounded open underground space such as underground mines and road/subway tunnels. In the former case, networks of wireless nodes are buried *underground* and communicate *through soil*. In this case, the WUCNs promise a wide variety of novel applications, including intelligent irrigation, environmental monitoring, infrastructure monitoring, localization, and border patrol [1]. In the latter case, although the network is located *underground*, the communication takes place *through the air*, i.e., through the voids that exist underground. In this case, the WUCNs are necessary to improve the safety and productivity in underground mines, to realize convenient communication for drivers and passengers in road/subway tunnels, and to avoid attacks by continuously monitoring these vulnerable areas.

The main challenge for WUCNs is the realization of efficient and reliable underground wireless links to establish multiple hops and disseminate data for seamless operation. The main difference between the WUCNs and the terrestrial wireless communication networks is the

* Corresponding author. Tel.: +1 404 894 5141; fax: +1 404 894 7883.
E-mail addresses: ian@ece.gatech.edu (I.F. Akyildiz), zsun@ece.gatech.edu (Z. Sun), mcvuran@cse.unl.edu (M.C. Vuran).

1874-4907/$ – see front matter © 2009 Elsevier B.V. All rights reserved.
doi:10.1016/j.phycom.2009.03.004

communication medium. For the WUCNs deployed in soil, the propagation medium is no longer air but soil, rock, and water. Although the well established terrestrial signal propagation techniques based on electromagnetic (EM) waves may still work in a soil medium, the channel model of EM waves in this environment needs to be developed. Besides EM waves, alternate signal propagation techniques, such as magnetic induction (MI) can also be used for short-range communication in soil. For the WUCNs deployed in underground mines and road/subway tunnels, the EM waves are the best choice for wireless signal propagation, since the radio signal propagates through the air in this case. However, the propagation characteristics of EM waves are significantly different from those of terrestrial wireless channels because of the restrictions caused by the lossy dielectric walls and ceilings in the underground mines or road/subway tunnels.

This paper analyzes the underground wireless signal propagation techniques and presents current research challenges of the WUCNs. More specifically, the following are provided:

Channel models for communication through soil: For WUCNs in soil, we provide a channel model for EM and MI waves. The former model characterizes not only the propagation of EM waves in soil, but also other effects such as multipath, soil composition, water content, and burial depth [2,3]. Our analysis shows that the communication success significantly depends on the operating frequency and the composition of the soil. For low depth deployments, the channel is shown to exhibit a two-path channel model with the effect of multi-path fading of spatial distribution. For high depth deployments, a single path channel is suitable to characterize communication. We also analyze the MI communication channel in the soil medium. Based on the channel model, the MI waveguide technique for communication is developed to address the high attenuation rate of MI signals through multi-hop communication [4,5].

Channel models for communication in underground mines and tunnels: For WUCNs in underground mines and road/subway tunnels, the channel model for the EM waves is developed in two categories: *tunnel* channel model and *room-and-pillar* channel model. We provide an analytical channel model, i.e., the *multimode model* [6, 7]. For a tunnel environment, the multimode model can completely characterize natural wave propagation in both near and far regions of the source. For the room-and-pillar environment, the multimode model is combined with the shadow fading model. Based on the new channel model, we present an in-depth analysis of the wireless channel characteristics in underground mines and road/subway tunnels.

Research challenges for WUCNs: The analysis of the signal propagation techniques in both the soil medium and the underground mines/tunnels lays out the foundations for efficient communication in these environments. Based on the analysis, research challenges to design communication protocols in both underground environments are discussed.

The remainder of this paper is organized as follows: In Section 2, the channel model and the evaluations for communication based on EM waves in a soil medium are presented. In Section 3, the magnetic induction (MI) communication channel in a soil medium is provided, and the MI waveguide technique for communication is developed. Then in Section 4, our solution for channel modeling in underground mines and road/subway tunnels is presented. Next in in Section 5, research challenges to design communication protocols for WUCNs are discussed. Finally, the paper is concluded in Section 6.

2. Wireless communication through soil using electromagnetic waves

EM waves encounter much higher attenuation in soil compared to air. This severely hampers the communication quality. Moreover, the ground surface causes reflection as well as refraction, which requires a comprehensive investigation of the channel model. In addition, multi-path fading is another important factor in underground communication, since unpredictable obstacles in soil such as rocks and roots of trees make EM waves refracted and scattered. Therefore, advanced models are necessary to accurately and completely characterize the underground channel and to lay out the foundations for efficient underground communication.

2.1. 2-path rayleigh fading channel model

For the derivation of the underground channel model, we first model the propagation characteristics in soil. Then, the effects of reflections from the ground surface and the multi-path fading are captured. Finally, the bit error rate (BER) is derived as a function of communication parameters such as operating frequency, modulation type, distance as well as soil parameters such as volumetric water content, sand and clay percentage, and temperature.

2.1.1. Signal propagation through soil

The propagation through soil is modeled based on the Friis free space propagation equation [8], where a correction factor is included to account for the effects of the soil medium. As a result, the received signal, P_r, at a receiver sensor node is modeled as

$$P_r = P_t + G_r + G_t - L_p, \tag{1}$$

where P_t is the transmit power, G_r and G_t are the gains of the receiver and transmitter antennae, $L_p = L_0 + L_s$, L_0 is the path loss in free space, and L_s stands for the additional path loss caused by the propagation in soil. The additional path loss, L_s, is calculated by considering the following differences of EM wave propagation in soil compared to that in air: (1) The signal velocity, and hence, the wavelength λ, is different, (2) the amplitude of the wave will be attenuated according to the frequency, and (3) the phase velocity is correlated with the frequency in the soil, which can cause color scattering and delay distortion. The additional path loss, L_s, in soil is, hence, composed of two components

$$L_s(dB) = L_\beta(dB) + L_\alpha(dB), \tag{2}$$

where L_β is the attenuation loss due to the difference of the wavelength of the signal in soil, λ, compared to the wavelength in free space, λ_0, and L_α is the transmission loss caused by attenuation with attenuation constant α.

Then, L_p can be represented in dB as follows [3]:

$$L_p = 6.4 + 20\log(d)(m) + 20\log(\beta) + 8.69\alpha d, \quad (3)$$

where distance, d, is given in meters, the attenuation constant, α, is in 1/m and the phase shifting constant, β, is in rad/m. Note that the path loss, L_p, in (3) depends on the attenuation constant, α, and the phase shifting constant, β, which depends on the dielectric properties of soil. Using the Peplinski principle [9], the dielectric properties of soil in the 0.3–1.3 GHz band can be calculated as follows:

$$\epsilon = \epsilon' - j\epsilon'',$$
$$\epsilon' = 1.15\left[1 + \frac{\rho_b}{\rho_s}(\epsilon_s^{\alpha'}) + m_v^{\beta'}\epsilon_{f_w}'^{\alpha'} - m_v\right]^{1/\alpha'} - 0.68,$$
$$\epsilon'' = [m_v^{\beta''}\epsilon_{f_w}''^{\alpha'}]^{1/\alpha'}, \quad (4)$$

respectively, where ϵ is the relative complex dielectric constant of the soil-water mixture, m_v is the volumetric water content (VWC) of the mixture, ρ_b is the bulk density in grams per cubic centimeter, $\rho_s = 2.66$ g/cm^3 is the specific density of the solid soil particles, $\alpha' = 0.65$ is an empirically determined constant, and β' and β'' are empirically determined constants, dependent on soil type and given by

$$\beta' = 1.2748 - 0.519S - 0.152C,$$
$$\beta'' = 1.33797 - 0.603S - 0.166C, \quad (5)$$

where S and C represent the mass fractions of sand and clay, respectively. The quantities ϵ'_{f_w} and ϵ''_{f_w} in (4) are the real and imaginary parts of the relative dielectric constant of water. Consequently, the attenuation constant, α, and the phase shifting constant, β, are found as

$$\alpha = \omega\sqrt{\frac{\mu\epsilon'}{2}\left[\sqrt{1 + \left(\frac{\epsilon''}{\epsilon'}\right)^2} - 1\right]},$$
$$\beta = \omega\sqrt{\frac{\mu\epsilon'}{2}\left[\sqrt{1 + \left(\frac{\epsilon''}{\epsilon'}\right)^2} + 1\right]}, \quad (6)$$

where $\omega = 2\pi f$ is the angular frequency, μ is the magnetic permeability, and ϵ' and ϵ'' are the real and imaginary parts of the dielectric constant as given in (4), respectively. Consequently, the path loss, L_p, in soil can be found by using Eqs. (4)–(6) in (3).

It can be seen from above equations that the complex propagation constant of the EM wave in soil is dependent on the operating frequency, the composition of the soil in terms of sand and clay fractions, S and C, the bulk density, ρ_b, and the volumetric water content (VWC), m_v. Consequently, the path loss, L_p, also depends on these parameters.

2.1.2. Reflection from ground surface

Underground communication results in two main paths for signal propagation as shown in Fig. 1. The first path is the direct path between two sensors and the second path is the reflection path due to the ground surface. When the bury depth increases to a certain degree, i.e., *high depth*, the effect of reflection can be neglected and the channel can be considered as a single path. In this case, the path loss is given in (3). However, if the sensors are buried near the surface of ground, i.e., *low depth*, the total path loss of a two-path channel model can be deduced as follows:

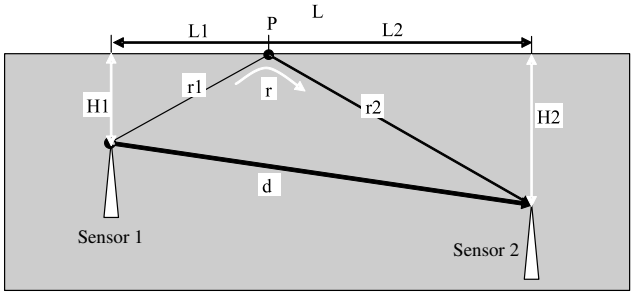

Fig. 1. Illustration of the two-path channel model.

$$L_f(dB) = L_p(dB) - V_{dB}, \quad (7)$$

where L_p is the path loss due to the single path given in (3) and V_{dB} is the attenuation factor due to the second path in dB, i.e., $V_{dB} = 10\log V$ and is given as follows:.

$$V^2 = 1 + (\Gamma \cdot \exp(-\alpha\Delta(r)))^2 - 2\Gamma\exp(-\alpha\Delta(r))\cos\left(\pi - \left(\phi - \frac{2\pi}{\lambda}\Delta(r)\right)\right), \quad (8)$$

where, Γ and ϕ are the amplitude and phase angle of the reflection coefficient at the reflection point P, $\Delta(r) = r - d$, is the difference of the two paths and α is the attenuation constant mentioned before. The effects of a two-path channel model have also been observed through our recent field experiments [10].

2.1.3. Multi-path fading

The two-path channel model captures the main propagation characteristics of EM waves underground. However, the surface of the ground is not ideally smooth and, hence, not only causes reflection, but also refraction. Moreover, usually, there are rocks or roots of plants in soil and the clay of soil is generally not homogeneous. As a result of the impurities in the soil, multi-path fading should also be considered in addition to the basic two-path channel model.

In underground communication, randomness in an underground environment is due to the locations of the nodes rather than time, which obeys the Rayleigh probability distribution. The only difference compared to communication through air is that the variable of Rayleigh probability distribution is location instead of time. Accordingly, we model each path in the underground channel such that the envelope of the signal is modeled as an independent Rayleigh distributed random variable, χ_i, $i \in \{1, 2\}$. Consequently, for the *single-path model*, the received energy per bit per noise power spectral density is given by $r = \chi^2 E_b/No$, which has a distribution as $f(r) = 1/r_0\exp(r/r_0)$, where $r_0 = E[\chi^2]E_b/N_o$ and E_b/N_o can be directly found from the signal-to-noise ratio (SNR) of the channel.

Similarly, for the *two-path model*, the received signal is the sum of two independent Rayleigh fading signals, which is denoted as *location dependent two path Rayleigh channel*. Consequently, the composite attenuation constant, χ, in

multi path Rayleigh channel is:

$$\chi^2 = \chi_1^2 + (\chi_2 \cdot \Gamma \cdot \exp(-\alpha\Delta(r)))^2 - 2\chi_1\chi_2\Gamma \exp(-\alpha\Delta(r)) \cos \times \left(\pi - \left(\phi - \frac{2\pi}{\lambda}\Delta(r)\right)\right), \quad (9)$$

where χ_1 and χ_2 are two independent Rayleigh distributed random variables of two paths, respectively. Γ and ϕ are the amplitude and phase angle of the reflection coefficient at the reflection point P, $\Delta(r) = r - d$, is the difference of the two paths and α is the attenuation constant. The relatively stable nature of the underground channel with respect to time has also been observed through our recent field experiments [10].

2.2. Characteristics of EM waves in soil

Based on the developed channel model, the bit error rate (BER) profile in underground settings can be evaluated. The BER of a communication system depends mainly on three factors: (1) the channel model (2) the signal-to-noise ratio (SNR), and (3) the modulation method used by the system. Considering the channel model derived before, the signal to noise ratio (SNR) is given by $SNR = P_t - L_f - P_n$, where P_t is the transmit power, L_f is the total path loss, and P_n is the noise energy. In the following part, we will discuss the effects of various factors on the BER in wireless channel of soil medium, including modulation method, operation frequency, deployment depth, transmit power, and volumetric water content.

2.2.1. Modulation scheme

In order to provide an initial investigation in this area, various modulation schemes including ASK, FSK and PSK are investigated to illustrate their effects on the BER [2]. The relation between the maximum inter-node distance of the single path channel model and the VWC is shown in Fig. 2(a). The maximum inter-node distance is found subject to a BER target of 10^{-3} for different modulation methods. In Fig. 2(a), it can be seen that the PSK modulation method provides the largest range. Consequently, in our analysis, we consider the PSK modulation.

2.2.2. Operation frequency and deployment depth

In Fig. 2(b), the path loss is shown as a function of the burial depth, H, for various values of the operating frequency, f. For a particular operating frequency, an optimum bury depth exists such that the path loss is minimized. This is particularly important in the topology design of WUCNs, where deployment should be tailored to the operating frequency of the wireless sensors. In Fig. 2(b), it can also be observed that the effect of reflection, and hence, the fluctuations in path loss diminishes as the bury depth, H, increases. More specifically, the underground channel exhibits a single-path characteristic when the bury depth is higher than 2 m since the influence of reflection is negligible. On the other hand, for low depth deployment, a two-path channel model should be considered.

2.2.3. Transmit power and volumetric water content

The effects of transmit power and the volumetric water content (VWC) on the BER are shown in Fig. 3, where the

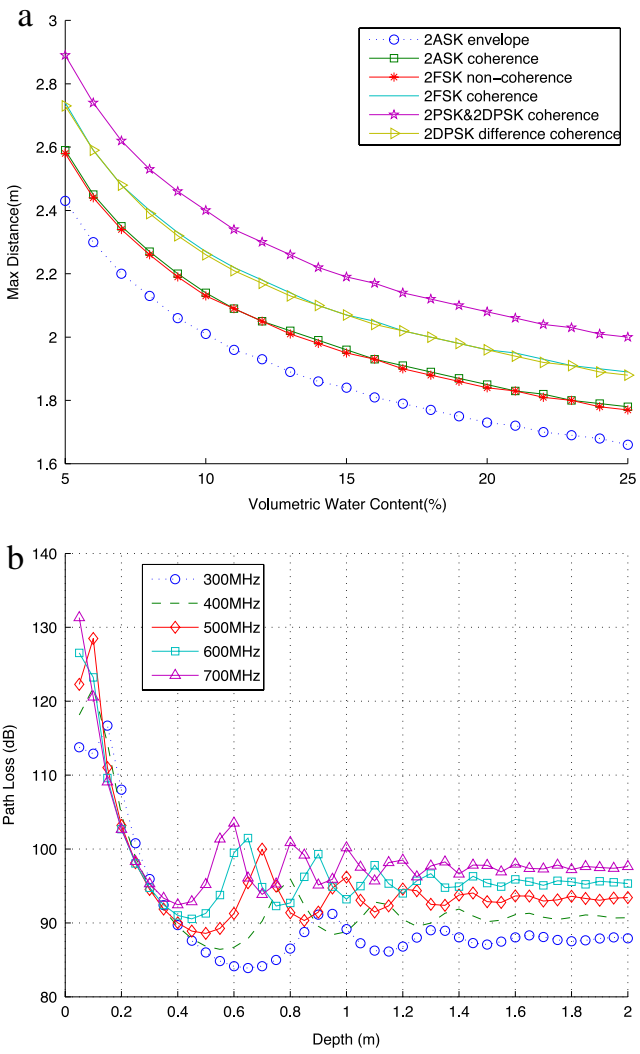

Fig. 2. (a) The maximum inter-node communication distance of one path channel using different modulation schemes. (b) Path loss vs. depth for different operating frequencies with two-path channel model.

results are shown for single-path and two-path models. In Fig. 3(a), the relation between BER and horizontal distance for different transmit power values is shown. It is observed that as the transmit power increases, the BER decreases. However, this decrease is a minimum since even when the transmit power increases to 30 dBm, the horizontal distance can only be extended to 4 m with the limitation that the BER is below 10^{-3}. As shown in Fig. 3(b), an increase in the VWC from 5% to 10% results in almost an order of magnitude increase in the BER. In addition to the theoretical analysis, our recent field experiments also illustrate the effect of the VWC [10]. These results confirm that *VWC is one of the most important parameters for underground communication.*

In Fig. 3, the effect of the reflected path from the ground surface on the BER can also be clearly seen through the 2-path model. As shown in Fig. 3(a), the BER results for the two-path model shifts to right compared to the one-path model. More specifically, the communication distance can be extended for low depth applications to 4.5–5 m with transmit power of 30 dBm with depth 0.5 m at 400 MHz. Finally, the effect of the VWC in two-path model is shown

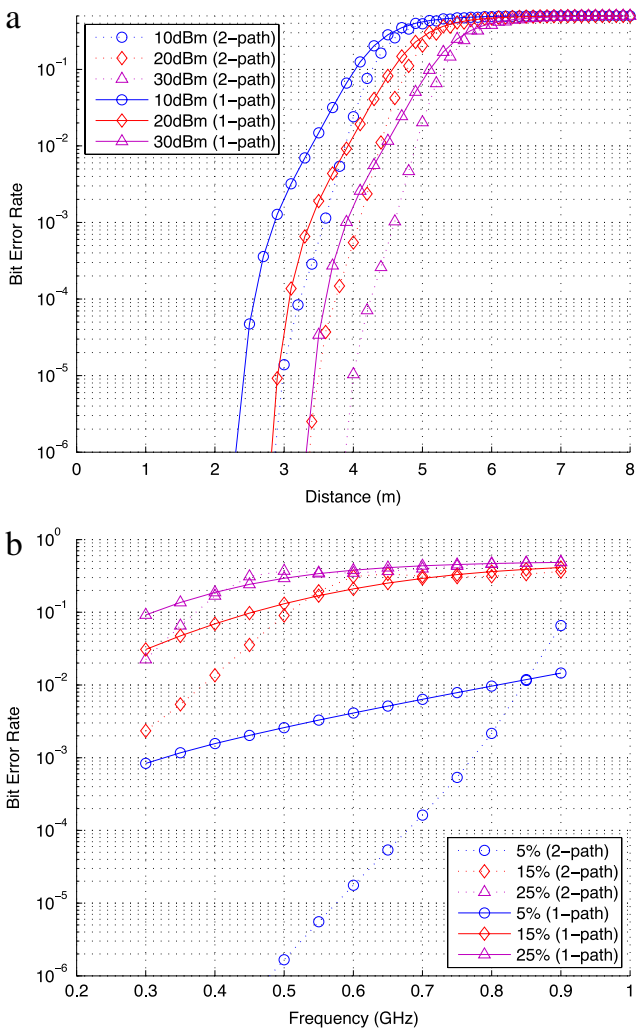

Fig. 3. (a) BER vs. internode distance with different transmitting power and (b) BER vs. operating frequency and volumetric water content for one-path and two-path channel models.

in Fig. 3(b). Compared to the single-path model results shown also in this figure, a higher VWC is acceptable for low depth deployments when the operation frequency is low.

2.2.4. Volumetric water content variation

The above analysis is performed assuming that the VWC is constant throughout the soil. However, field measurements reveal that the VWC also changes with depth [11–13]. Moreover, even at the same depth, communication range can change by as much as 25% depending on the time of the year. To investigate the relation between communication quality and the burial depth, the BER is evaluated based on the experimental data in [13,12]. We denote these data sets as *Set* 1 and *Set* 2, where the properties of each experiment are described as follows:

- *Set* 1: The first data set consists of volumetric water content values measured at different depths in a black soil with 22.75% sand, 28.1% clay [13].
- *Set* 2: The second data set is from a sandy soil with 50% sand and 15% clay [12]. Since sandy land soil keeps less water compared to the black soil, this data set was included to illustrate the effect of soil content on the influence of variation of the VWC on communication range.

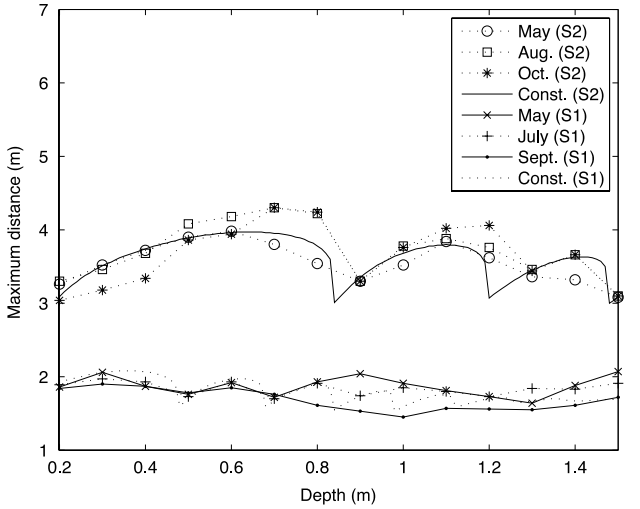

Fig. 4. The maximum inter-node distance vs. depth for the data Set 1 (S1) and Set 2 (S2) at different times of the year. Maximum distance calculated by considering a constant VWC at all depths is also shown.

The maximum inter-node communication distance is calculated for these two data sets. In Fig. 4, the maximum inter-node distance for the BER target of 10^{-3} is shown as a function of depth for both data sets. The solid lines represent the cases where the VWC is considered constant throughout all depths for each data set. For Set 1, $VWC = 20\%$, which is the value measured at 0.3 m depth in May according to [13] and for Set 2, $VWC = 3.7\%$. When Set 1 is considered, it can be observed that the fluctuations estimated by the uniform VWC model are closely followed when the depth is $d \leq 0.8$ m.

The seasonal influence on communication is also shown in Fig. 4. Especially, for burial depths higher than 0.8 m, the communication range is higher during May and lower during September compared to the uniform VWC case. This is related to higher precipitation, which starts in July. The results in Fig. 4 reveal that even at the same depth, the communication range can change by as much as 25% depending on the time of the year. Consequently, environmental adaptive protocols, which can adjust the operating parameters according to the seasons, are necessary for robust operation in WUCNs.

3. Wireless communication through soil using magnetic induction

As discussed in Section 2, traditional signal propagation techniques using EM waves encounter three major problems in soil medium: high path loss, dynamic channel condition and large antenna size [2]. First, EM waves experience high levels of attenuation due to absorption by soil, rock, and water in the underground. Second, the path loss is highly dependent on numerous soil properties such as water content, soil makeup (sand, silt, or clay) and density, and can change dramatically with time (e.g., increased soil water content after rainfall) and space (soil properties change dramatically over short distances). Consequently,

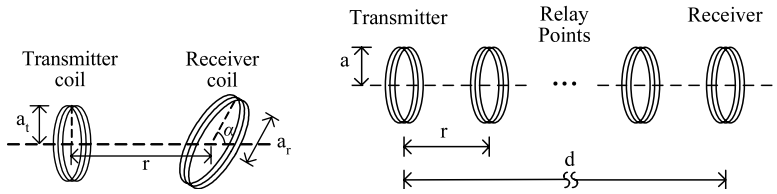

Fig. 5. The structure of the MI transceiver and the MI waveguide.

the bit error rate (BER) of the communication system also varies dramatically in different times or positions. An unreliable channel brings design challenges for the underground devices and networks to achieve both satisfying connectivity and energy efficiency. Third, operating frequencies in MHz or lower ranges are necessary to achieve a practical transmission range [1]. To efficiently transmit and receive signals at that frequency, the antenna size is too large to be deployed in the soil.

Magnetic induction (MI) is an alternative signal propagation technique for underground wireless communication, which addresses the dynamic channel condition and large antenna size challenges of the EM wave techniques. In particular, a dense medium such as soil and water causes little variation in the attenuation rate of magnetic fields from that of air, since the magnetic permeabilities of each of these materials are similar [1,14,15]. Therefore the MI channel conditions remain constant in a soil medium. Moreover, in the MI communication, the transmission and reception are accomplished with the use of a small coil of wire. Therefore, no lower limit of the coil size is required. However, the magnetic field strength falls off much faster than the EM waves [16,17]. Consequently, MI is generally unfavorable for terrestrial wireless communication. In a soil medium, although the path loss of MI caused by the soil absorption is much less than the EM waves, the total path loss may still be higher.

In this section, we first derive the analytical expression of the path loss of the underground MI communication channel. Multiple factors are considered in the analysis, including the soil properties, coil size, the number of turns in the coil loop, coil resistance and operating frequency. To reduce the high path loss and extend the transmission range, we develop the MI waveguide technique [4,5] for underground wireless communication. The MI waveguide has three advantages in underground wireless communication: first, by carefully designing the waveguide parameters, the path loss can be greatly reduced. Second, the relay coils constituting the MI waveguide do not consume any energy and the cost is very small. Third, the MI waveguide is not a continuous structure like a real waveguide hence it is relatively flexible and easy to deploy and maintain. We compare the performance of the traditional EM wave systems, the current MI systems and our improved MI waveguide system. It is shown in the results that our MI waveguide system has a much lower path loss than the other two systems for any channel conditions.

3.1. MI channel model

In MI communication, the transmission and reception are accomplished with the use of a coil of wire, as shown in Fig. 5(a), where a_t and a_r are the radii of the transmission coil and receiving coil, respectively; r is the distance between the transmitter and the receiver; and $(90° - \alpha)$ is the angle between the axes of two coupled coils.

The ratio of the received power to the transmitting power, i.e. the path loss, is [4,5]:

$$\frac{P_r}{P_t} \simeq \frac{\omega^2 \mu^2 N_t N_r a_t^3 a_r^3 \sin^2 \alpha}{8r^6} \cdot \frac{1}{4R_0(2R_0 + \frac{1}{2}j\omega\mu N_t)} \tag{10}$$

where N_t and N_r are the number of turns of the transmitter coil and receiving coil, respectively; R_0 is the resistance of a unit length of the loop; μ is the permeability of the medium (i.e., soil); and ω is the angle frequency of the transmitting signal. If a low-resistance loop, high signal frequency and a large number of turns are employed ($\omega\mu N_t \gg R_0$), then the ratio can be further simplified:

$$\frac{P_r}{P_t} \simeq \frac{\omega\mu N_r a_t^3 a_r^3 \sin^2 \alpha}{16R_0 r^6}. \tag{11}$$

According to (11), the received power loss is a 6th-order function of the transmission range r. A higher signal frequency ω, a larger number of turns N, lower loop resistance R_0 and a larger coil size a can enlarge the received power. The angle between the axes of the two coupled coils also affects the received power: the smaller the angle is, the higher the power that is received. It should be noted that the received power is not affected by the environmental conditions. It is because only one environment parameter μ exists in (11) and the permeability μ of soil and water is similar to that of air.

We compare (11) with the Friis transmission equation for the EM wave communication [18], where

$$\frac{P_r}{P_t} \simeq G_t G_r \left(\frac{\lambda}{4\pi r}\right)^2 = G_t G_r \frac{\pi}{4\mu\varepsilon\omega^2 r^2}. \tag{12}$$

It shows that a higher operating frequency induces a higher path loss in the EM wave case but achieves a lower attenuation rate in the MI case. The received power of MI communication attenuates much faster than the EM wave case ($1/r^6$ vs. $1/r^2$). However, the permittivity ε in (12) is much larger in soil than that in air. Furthermore, ε varies a lot at different times and locations. Hence, the path loss of EM waves is dramatically influenced by those environmental conditions. Accordingly, the MI technique has a constant channel condition while the EM wave technique results in lower attenuation.

3.2. MI waveguide

Although the MI techniques address the dynamic channel condition and large antenna size challenges of

the EM wave techniques, its received power loss is much higher than in the EM wave case. For practical applications, this can be addressed by employing relay points between the transmitter and the receiver.

Contrary to the relay points used for the EM waves, the MI relay point is a simple coil without any energy source or processing device. The sinusoidal current in the transmitter coil induces a sinusoidal current in the first relay point. This sinusoidal current in the relay coil then induces another sinusoidal current in the second relay point, and so on and so forth. These relay coils form an MI waveguide in underground environments, which act as a waveguide that guides the so-called *MI waves*.

A typical MI waveguide structure is shown in Fig. 5(b), where, n relay coils are equally spaced along one axis between the transmitter and the receiver; r is the distance between neighboring coils; d is the distance between the transmitter and the receiver and $d = (n+1)r$; a is the radius of the coils. In fact, there exists mutual induction between any pair of the coils. The value of the mutual induction depends on how close the coils are to each other. For the MI waveguide model developed in this section, the distance between two relay coils is assumed to be around 1 m and the coil radius is no more than 0.1 m. Therefore we assume that the coils are sufficiently far from each other and only interact with the nearest neighbors. Hence, only the mutual induction between the adjacent coils needs to be taken into account.

The path loss of the MI waveguide is given as [4,5]:

$$\frac{P_r}{P_t} \simeq \frac{\omega^2\mu^2N^2a^6}{8r^6}\frac{1}{4R_0\left(2R_0+\frac{1}{2}j\omega\mu N\right)} \times\left[\frac{j}{\frac{4R_0}{\omega\mu N}\left(\frac{r}{a}\right)^3+j\left(\frac{r}{a}\right)^3+\frac{\omega\mu N}{4R_0+j\omega\mu N}\left(\frac{a}{r}\right)^3}\right]^{2n}. \quad (13)$$

Under the condition that a high signal frequency and a large number of turns are employed ($\omega\mu N \gg R_0$), Eq. (13) can be further simplified:

$$\frac{P_r}{P_t} \simeq \frac{\omega\mu N}{16R_0}\left(\frac{a}{r}\right)^{6n} = \frac{\omega\mu N}{16R_0}\left[\frac{a}{d}(n+1)\right]^{6n}. \quad (14)$$

It is shown in (14) that the transmission range d is divided into $n+1$ intervals with length r. However, the path loss becomes a $6n$th-order function of the relay interval r. Hence, to reduce the path loss of the MI waveguide, the relay interval r needs to be on par with the coil size to make the term a/r approximately 1. It means that if coils with a radius of 0.1 m are utilized, we need to deploy this kind of coil every 0.1 m, which is infeasible in underground communications considering the deployment difficulty. Consequently, simple relay coils cannot reduce the path loss.

By analyzing (13), we find that if the last term with exponent $2n$ converges to a value around 1, the MI waveguide path loss can be greatly reduced. Fortunately, we can achieve this goal by adding a capacitor in each coil and carefully designing the capacitor value, the operating frequency and the number of turns in the coil. We assume that each coil is loaded with a capacitor C, then the ratio of the received power to the transmitting power of the MI waveguide is:

$$\frac{P_r}{P_t} = \frac{\omega^2\mu^2N^2a^6/4r^6}{\left(2R_0+j\frac{\omega\mu N}{2}+\frac{1}{j\omega CN\pi a}\right)\left(4R_0+\frac{\omega^2\mu^2N^2a^6/4r^6}{2R_0-j\frac{\omega\mu N}{2}-\frac{1}{j\omega CN\pi a}}\right)} \times\left[\frac{j}{\frac{4R_0r^3}{\omega\mu Na^3}+j\left(\frac{r}{a}\right)^3-j\frac{2\left(\frac{r}{a}\right)^3}{\omega^2\mu CN^2\pi a}+\frac{\omega\mu N\left(\frac{a}{r}\right)^3}{4R_0+j\omega\mu N+\frac{2}{j\omega CN\pi a}}}\right]^{2n}. \quad (15)$$

By assigning the capacitor C an appropriate value, the self-induction term can be neutralized. Then the term with exponent $2n$ can be greatly diminished. Specifically, we set the value of the capacitor C to be:

$$C = \frac{2}{\omega^2N^2\mu\pi a}. \quad (16)$$

Then the MI waveguide path loss becomes:

$$\frac{P_r}{P_t} = \frac{\omega^2\mu^2N^2a^6/4r^6}{2R_0\left(4R_0+\frac{\omega^2\mu^2N^2a^6}{2R_0\cdot 4r^6}\right)} \times\left[\frac{j}{\frac{4R_0}{\omega\mu N}\left(\frac{r}{a}\right)^3+\frac{\omega\mu N}{4R_0}\left(\frac{a}{r}\right)^3}\right]^{2n}. \quad (17)$$

After that, the operating frequency and the number of turns are designed to further reduce the path loss. In particular, if

$$\frac{\omega\mu N}{4R_0}\left(\frac{a}{r}\right)^3 = 1, \quad (18)$$

then

$$\frac{P_r}{P_t} = \frac{1}{3}\left(\frac{1}{2}\right)^{2n}. \quad (19)$$

From (19), we find that the MI waveguide path loss is greatly reduced compared with current MI techniques and traditional EM wave techniques. The path loss is a function of the number of the relay points n. A larger n may cause a higher path loss. n is determined by the transmission distance d and the relay interval r. The longer r is, the lower the path loss would be. r is expected to be as large as possible but restricted by (16) and (18). Specifically, in (18), the relay interval r and the coil size a determine the operating frequency ω and the number of turns N. In (16), the capacitor value C is determined by a, N and ω. Hence, when designing the relay interval, we need to guarantee that the operating frequency, the number of turns and the capacitor value can be assigned feasible and appropriate values. We assume that the operating frequency is several hundred MHz and the coil radius is 0.1 m. Under these conditions, the relay interval around 1 m can satisfy the above requirements.

3.3. Characteristics of MI waves and MI waveguide in soil

We use MATLAB to quantitatively compare the path loss of the traditional EM wave technique, the current MI

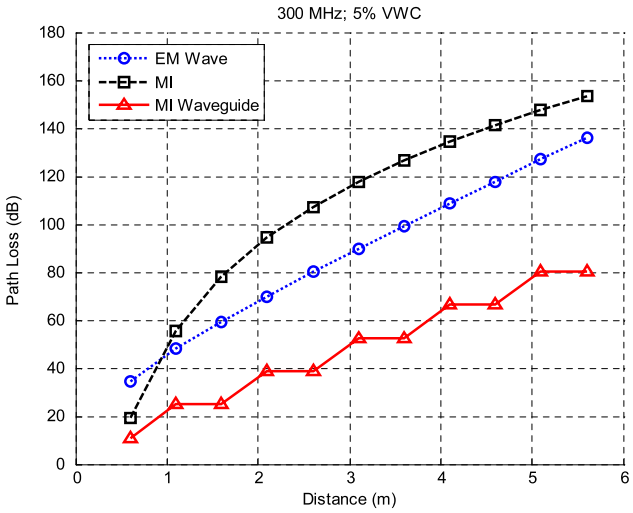

(a) 300 MHz signal in soil with 5% VWC.

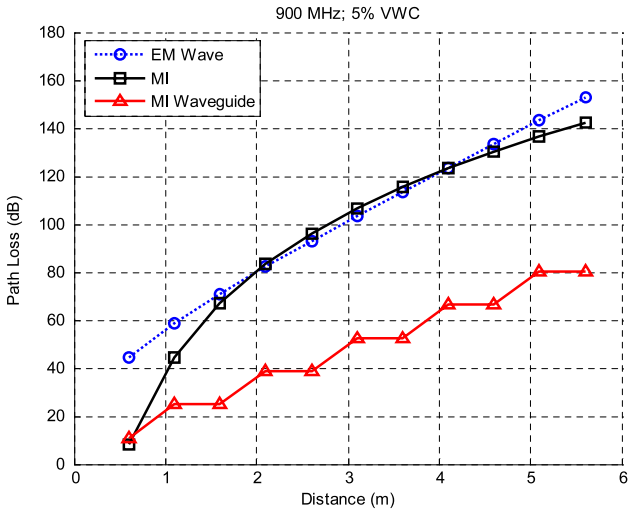

(b) 900 MHz signal in soil with 5% VWC.

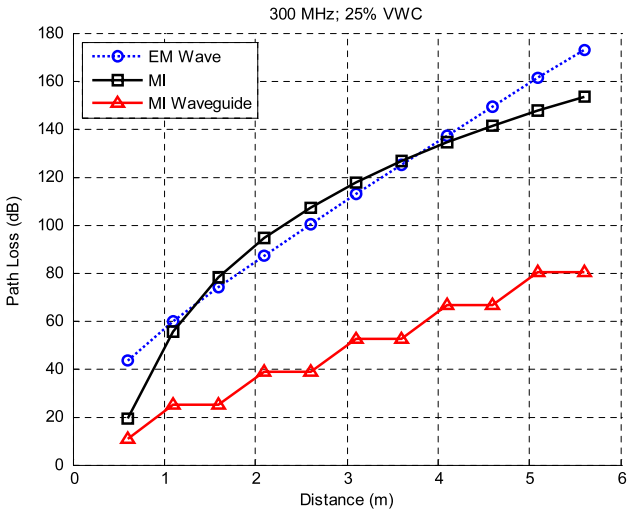

(c) 300 MHz signal in soil with 25% VWC.

Fig. 6. Path loss of the three techniques using different operating frequency in soil with different VWC.

technique and the improved MI waveguide technique for wireless underground communication. The channel model developed in [2,3] is utilized to describe the EM wave propagation in soil. For MI and MI waveguide systems, the models described in Eqs. (11) and (19) are used.

Except for studying the effects of certain parameters, the default values are set as follows: the volumetric water content (VWC) is 5% and the operating frequency is 300 MHz. The transmitter, receiver and relay coil all have the same radius of 0.1 m. The coil is made of copper wire with a 0.5 mm diameter hence the resistance of a unit length R_0 is 0.216 Ω/m. The permeability of the soil medium is the same as that in air, which is $4\pi \times 10^{-7}$ H/m. The relay interval r of the MI waveguide is 1 m. The number of relay coils n is determined by the transmission distance d, where $n = \lceil d/r \rceil$. The coil capacity is calculated by (16), which is around 20 pF.

3.3.1. Low operating frequency and low volumetric water content

Fig. 6(a) shows the path loss of the three techniques in dB versus the transmission distance d using a 300 MHz signal in soil with a 5% VWC. It can be seen that in the very near region ($d < 1$ m), the path loss of the MI technique is smaller than that of the EM wave technique. However, as the transmission distance increases, the MI signal attenuates much faster than the EM wave signal. It may have up to 20 dB higher path loss than the EM wave signal. As expected, the MI waveguide technique greatly reduces the signal path loss compared to the other two techniques. It is shown that the path loss of the MI waveguide system is less than 50% of the MI and EM wave cases in a certain range.

3.3.2. High operating frequency and low volumetric water content

In Fig. 6(b), the VWC of soil remains the same but the operating frequency is increased to 900 MHz. On one hand, the path loss of the EM wave system slightly increases. The increase can be explained by (12) where the operating frequency ω is in the denominator. Because the material absorption is the major part of the EM wave path loss in soil, the attenuation caused by the higher operating frequency is not dramatic. On the other hand, the path

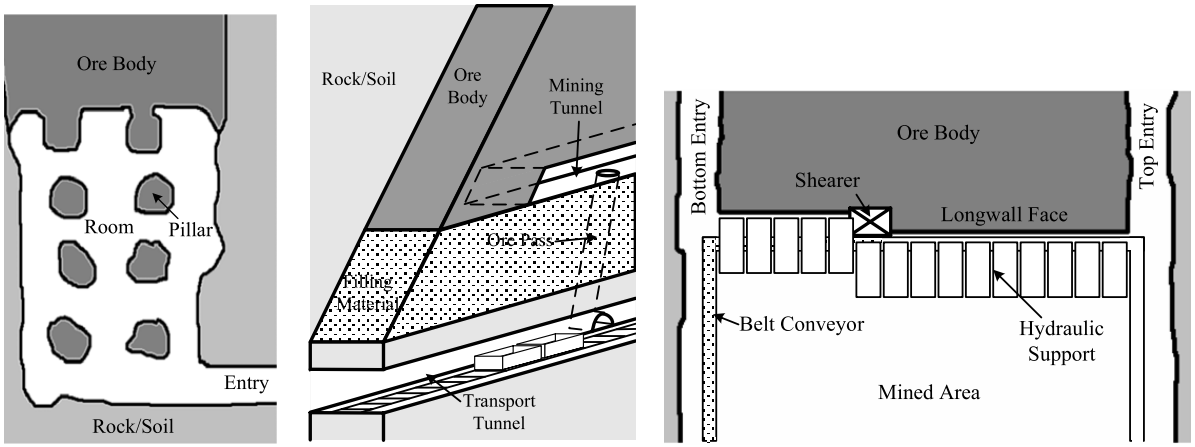

(a) Room-and-pillar mining. (b) Cut-and-fill mining. (c) Longwall mining.

Fig. 7. Mine structure of different mining methods.

loss of the MI system decreases as the operating frequency increases, which can be explained by Eq. (11) where the operating frequency ω is in the numerator. Hence it can be concluded that with a high operating frequency, the path loss of the EM wave system becomes higher than that of the MI system. The path loss of the MI waveguide system remains the lowest when a high operating frequency is used. As discussed previously, the operating frequency does not affect the path loss but will influence the design of the capacitor value and the number of turns of the coil. A higher operating frequency requires a lower number of turns or lower capacitor value.

3.3.3. Low operating frequency and high volumetric water content

In Fig. 6(c), the influence of the underground environment on the three propagation techniques are analyzed. As discussed previously, the performance of MI and MI waveguide systems is not affected by the environment since the permeability μ remains the same, no matter whether the medium is air, water or soil. According to the channel models of EM waves in soil [2,3], the water content is the major environmental parameter that influences the EM wave propagation in soil. Therefore, we investigate the path loss of the three techniques in soil with a higher water content (25% VWC) in Fig. 6(c). As expected, the path loss of the MI and MI waveguide system remain the same as that in soil with a lower water content. However, the path loss of the EM wave system increases dramatically (up to 40 dB) in soil with a higher water content.

4. Wireless communication in underground mines and road/subway tunnels

In addition to deployments in soil, WUCNs can also be deployed in underground mines and road/subway tunnels. Although the EM waves actually propagate through the air in this case, the propagation characteristics of EM waves are significantly different from those of the terrestrial wireless channels because of the restrictions caused by the structures of the underground mines and road/subway tunnels. In underground mines, multiple passageways are developed to connect the aboveground entrance and different mining areas. The structure of the mining area is determined by mining methods, which is influenced by the shape and position of the ore body [19]:

- If the ore body is flat, room-and-pillar mining can be implemented as shown in Fig. 7(a). The mining area can be viewed as a big room with randomly shaped pillars in it.
- If the ore body has a steep dip, cut-and-fill mining, sublevel stoping or shrinkage stoping can be employed. Mines using those techniques have similar structures: the mining area consists of several types of tunnel, e.g. mining tunnel and transport tunnel. The sectional plan of cut-and-fill mining is shown in Fig. 7(b).
- If the ore body has a large, thin, seam-type shape, longwall mining is preferred as shown in Fig. 7(c). Besides the entry tunnels, the mining area near the longwall face can also be modeled as a tunnel since it is encircled by the hydraulic support and the longwall face.

According to the different structures of underground mines, two types of channel model are required. The *tunnel channel model* is used to describe the signal propagation in passageways and mining area tunnels. The *room-and-pillar channel model* characterizes the wireless channel of the room-and-pillar mining area. The structure of road/subway tunnels is similar to that of underground mine tunnels and can be captured through the tunnel channel model.

In this section, we develop an analytical channel model, the *multimode model*, which lays out the foundation for reliable and efficient communication networks in underground mines and road tunnels [6,7]. For the tunnel environment, the multimode model can completely characterize the natural wave propagation in both near and far regions of the transmitter. For the room-and-pillar environment, the multimode model is combined with the shadow fading model to characterize the random effects of the pillars in underground mines.

4.1. Multimode model for tunnel environments

To address the problems of the current tunnel channel models, we develop the multimode model, which can be regarded as a multi-mode operating waveguide model. The waveguide model [20] considers the modes that are all the possible solutions for the Maxwell's equations. Hence, only

the EM waves that have the same shapes as those modes can exist in the tunnel. However, the intensity of each mode depends on the excitation [21,22], which cannot be captured by the waveguide model. Therefore, the GO model [23] is exploited to analyze the EM field distribution for the excitation plane, i.e., the tunnel cross-section that contains the transmitter antenna. This field distribution can be considered as the weighted sum of the field of all modes. Hence, the intensity of each mode can be estimated by a mode-matching technique. Once the mode intensity is determined in the excitation plane, the propagation of each mode is mostly governed by the tunnel itself. Hence the EM field of the rest of the tunnel can be accurately predicted by summing the EM field of each mode.

4.1.1. Tunnel environment model

Although actual tunnel cross sections are usually in-between a rectangle and a circle, the EM field distribution and attenuation of the modes in rectangle waveguide are almost the same as a circular waveguide [24]. Hence, in our model, the tunnel cross section is treated as an equivalent rectangle with a width of $2a$ m and a height of $2b$ m. A Cartesian coordinate system is set with its origin located at the center of the rectangle tunnel. k_v, k_h and k_a are the complex electrical parameters of the tunnel vertical/horizontal walls and the air in the tunnel, respectively, which are defined as: $k_v = \varepsilon_0\varepsilon_v + \frac{\sigma_v}{j\omega}$, $k_h = \varepsilon_0\varepsilon_h + \frac{\sigma_h}{j\omega}$, $k_a = \varepsilon_0\varepsilon_a + \frac{\sigma_a}{j\omega}$, where ε_v, ε_h and ε_a are the relative permittivity for vertical/horizontal walls and the air in the tunnel; ε_0 is the permittivity in vacuum space; σ_v, σ_h and σ_a are their conductivity; ω is the angular frequency of the signal. The three areas are assumed to have the same permeability μ_0. The wave number in the tunnel space is given by $k = \omega\sqrt{\mu_0\varepsilon_0\varepsilon_a}$. We define the relative electrical parameter $\overline{k_v} = k_v/k_a$ and $\overline{k_h} = k_h/k_a$ for a concise expression.

4.1.2. Field analysis of excitation plane by GO model

The transmitter antenna is assumed to be an X-polarized electrical dipole. The total field of a point in the excitation plane is equal to the sum of ray contributions from all reflection images added to that of the source. The reflection images are located as Fig. 8 shows. Due to the geometry characteristic of rectangle cross section shape, the images and the reflection rays have the following properties:

- The ray coming from image $I_{p,q}$ experiences $|p|$ times reflection from the vertical wall and $|q|$ times reflection from the horizontal wall.
- Suppose that α is the incident angle on the horizontal wall, and β is the incident angle on the vertical wall. Then α and β are complementary. These angles remain the same for all reflections of a certain ray.

Consider that the transmitter antenna is located at the coordinate (x_0, y_0). The major polarized field, i.e. the X-polarized field, at the receiver is given by:

$$E_x^{Rx} = E_x^{Tx} \cdot \sum_{p,q} \left[\frac{\exp(-jkr_{p,q})}{r_{p,q}}\right] \cdot S(\overline{k_v})^{|p|} \cdot R(\overline{k_h})^{|q|} \tag{20}$$

where, E_x^{Tx} and E_x^{Rx} are the electric field at the transmitter and the receiver respectively; $r_{p,q}$ is the distance between image $I_{p,q}$ and the receiver; $R(\overline{k_h})$ and $S(\overline{k_v})$ are the reflection coefficients on the horizontal and vertical walls.

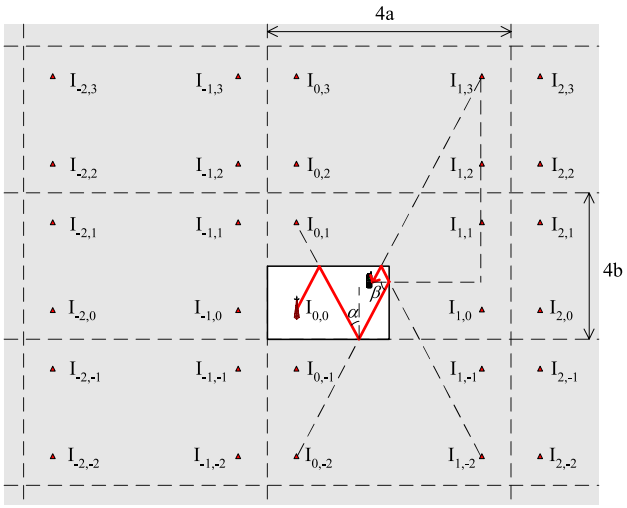

Fig. 8. The set of images in the excitation plane in a rectangular tunnel.

4.1.3. Mode-matching in excitation plane

The major field eigenfunctions of X-polarized modes $E_{m,n}^x$ are given by [25]. It has been pointed out that the modes in a rectangular tunnel are approximately orthogonal [26,27], i.e.

$$\int_{-a}^{a}\int_{-b}^{b} E_{m,n}^x \cdot E_{j,k}^{x*}\mathrm{d}x\mathrm{d}y \simeq \begin{cases}\xi^2, & \text{if } m=j \text{ and } n=k\\ 0, & \text{otherwise}\end{cases} \tag{21}$$

where ξ is the norm of the modes.

The field of the modes can be viewed as a basis that spans the total field. Therefore, the mode intensity C_{mn} can be calculated by projecting the field of the excitation plane obtained by the GO model (E_x^{Rx} in (20)) on the basis function $E_{m,n}^x$:

$$C_{mn} = \int_{-a}^{a}\int_{-b}^{b} E_x^{Rx} \cdot E_{m,n}^x \mathrm{d}x\mathrm{d}y. \tag{22}$$

4.1.4. Analytical solution for multimode model

Substitute (20) into (22) and change the sequence of summation and integration,

$$C_{mn} = \sum_{p,q}\left[\int_{-a}^{a}\int_{-b}^{b} E_x^{Rx}(p,q) \cdot E_{m,n}^x \mathrm{d}x\mathrm{d}y\right] \tag{23}$$

where, $E_x^{Rx}(p,q)$ is the field contributed by image $I_{p,q}$,

$$E_x^{Rx}(p,q) = E_x^{Tx} \cdot \frac{\exp(-jkr_{p,q})}{r_{p,q}} \cdot S(\overline{k_v})^{|p|} \cdot R(\overline{k_h})^{|q|}. \tag{24}$$

Then the mode intensity C_{mn} can be viewed as the sum of all the contributions of images: $C_{mn} = \sum_{p,q\in\mathbf{Z}} C_{mn}^{(p,q)}$, where,

$$C_{mn}^{(p,q)} = \int_{-a}^{a}\int_{-b}^{b}\left\{E_x^{Tx} \cdot \frac{\exp(-jkr_{p,q})}{r_{p,q}} \cdot S(\overline{k_v})^{|p|} \times R(\overline{k_h})^{|q|} \cdot E_{m,n}^x\right\}\mathrm{d}x\mathrm{d}y. \tag{25}$$

Divide the absolute mode intensity by the norm of the basis ξ and the field of reference position $E_x(r_0)$ (r_0 apart from the antenna), then we can obtain the normalized mode intensity:

$$\overline{C_{mn}^{(p,q)}} = \frac{C_{mn}^{(p,q)}}{\xi \cdot E_x(r_0)} = \frac{C_{mn}^{(p,q)}}{\xi \cdot E_x^{Tx} \cdot \frac{\exp(-jkr_0)}{r_0}} \simeq \frac{1}{\xi}\int_{-a}^{a}\int_{-b}^{b} \frac{r_0 \exp(-jkr_{p,q})}{r_{p,q}+r_0} S(\overline{k_v})^{|p|} R(\overline{k_h})^{|q|} \times E_{m,n}^{x} \mathrm{d}x\mathrm{d}y. \quad (26)$$

The closed form solution of the (26) is derived by composite numerical integration, which is given by:

$$\overline{C_{mn}^{(p,q)}} \simeq \frac{4}{3}\frac{\sqrt{ab}}{mn}\sum_{u=0}^{m-1}\sum_{v=0}^{n-1}\left\{\frac{r_0 \exp(-jkr_{p,q})}{r_{p,q}+r_0} S(\overline{k_v})^{|p|} R(\overline{k_h})^{|q|} \times (-1)^{\lfloor \frac{m+n}{2} \rfloor + 1 + u + v}\right\}. \quad (27)$$

The mode intensity is the summation of all contributions of the images, however only the low-order images have a significant effect. Specifically, for an X-polarized field, only images $I_{p,q}$ with subscript $p = 0, \pm 1$ and $q = 0, \pm 1, \pm 2$ are considered. In addition, to reduce the computation cost, the reflection coefficients R and S are simplified to their approximate expressions by non-linear regression. Therefore, the normalized intensity for an mn-order mode is:

$$\overline{C_{mn}} \simeq \frac{4}{3}\frac{\sqrt{ab}}{mn}\sum_{\substack{p=0,\pm1\\ q=0,\pm1,\pm2}}\left\{\sum_{u=0}^{m-1}\sum_{v=0}^{n-1}\left[\frac{r_0 \exp(-jkr_{p,q})}{r_{p,q}+r_0} S^{|p|} R^{|q|} \times (-1)^{\lfloor \frac{m+n}{2} \rfloor + 1 + u + v}\right]\right\} \quad (28)$$

where,

$$R^{|q|} = (-1)^{|q|}\exp\left(-2|q| \cdot \frac{y_q}{r_{p,q}\sqrt{\overline{k_h}}}\right)$$

$$S^{|p|} = \begin{cases} 1, & \text{if } p = 0 \\ 1 - 2 \cdot \dfrac{1}{1 + \frac{x_p}{r_{p,q}}\sqrt{\overline{k_v}}}, & \text{if } p = \pm 1 \end{cases}$$

$$x_p = \begin{cases} \left|2pa - x_0 + a - \dfrac{2a}{m}\left(u + \dfrac{1}{2}\right)\right|, & \text{if } p \text{ is odd} \\ \left|2pa + x_0 + a - \dfrac{2a}{m}\left(u + \dfrac{1}{2}\right)\right|, & \text{if } p \text{ is even} \end{cases}$$

$$y_q = \begin{cases} \left|2qb - y_0 + b - \dfrac{2b}{n}\left(v + \dfrac{1}{2}\right)\right|, & \text{if } q \text{ is odd} \\ \left|2qb + y_0 + b - \dfrac{2b}{n}\left(v + \dfrac{1}{2}\right)\right|, & \text{if } q \text{ is even} \end{cases}$$

$$r_{p,q} = \sqrt{x_p^2 + y_q^2}.$$

Then, the predicted field at any position (x, y, z) inside the tunnel can be obtained by summing up the field of all significant modes at that position, which is given by:

$$E_x^{Rx}(x, y, z) = E_x(r_0)\sum_{m,n}\overline{C_{mn}} \cdot E_{m,n}^{x}(x, y) \cdot \mathrm{e}^{-(\alpha_{mn} + j\beta_{mn})\cdot z} \quad (29)$$

where, α_{mn} is the attenuation coefficient and β_{mn} is the phase-shift coefficient [28,20,25]:

$$\alpha_{mn} = \frac{1}{a}\left(\frac{m\pi}{2ak}\right)^2 \mathrm{Re}\frac{\overline{k_v}}{\sqrt{\overline{k_v} - 1}} + \frac{1}{b}\left(\frac{n\pi}{2bk}\right)^2 \mathrm{Re}\frac{1}{\sqrt{\overline{k_h} - 1}}$$

$$\beta_{mn} = \sqrt{k^2 - \left(\frac{m\pi}{2a}\right)^2 - \left(\frac{n\pi}{2b}\right)^2}. \quad (30)$$

Similarly, the predicted received signal power at the coordinate (x, y, z) is given by:

$$P_r(x, y, z) = P_t G_t G_r \times \left(\frac{1}{2kr_0}\sum_{m,n}\overline{C_{mn}} \cdot E_{m,n}^{x}(x, y) \cdot \mathrm{e}^{-(\alpha_{mn} + j\beta_{mn})\cdot z}\right)^2 \quad (31)$$

where, P_t is the transmitting power; G_t and G_r are the antenna gains of the transmitter and the receiver, respectively.

The propagation delay of EH_{mn} mode is $\tau_{(mn)} = z/v_{g(mn)}$, where $v_{g(mn)}$ is the group velocity that is given by $v_{g(mn)} = c^2\beta_{mn}/2\pi f$. The RMS delay spread τ_{rms} is the standard deviation of the delay of all the modes, weighted proportional to the mode power:

$$\tau_{rms}^2 = \frac{\sum_{m,n}(\tau_{(mn)} - \tau_m)^2 P_{mn}(x, y, z)}{\sum_{m,n} P_{mn}(x, y, z)} \quad (32)$$

where, τ_m is the mean propagation delay at the position (x, y, z), and $P_{mn}(x, y, z)$ is the power coefficient of EH_{mn} mode at the position (x, y, z), given by:

$$P_{mn}(x, y, z) = \left|\overline{C_{mn}} \cdot E_{m,n}^{x}(x, y) \cdot \mathrm{e}^{-\Gamma_{mn}^{x}\cdot z}\right|^2. \quad (33)$$

4.2. Multimode model for room & pillar environments

The room-and-pillar environment can be regarded as a planar air waveguide superimposed with randomly distributed and random shaped pillars. A simplified multimode model is able to describe the EM wave propagation in the planar air waveguide. The randomly distributed and random shaped pillars form an environment very similar to a terrestrial metropolitan area with many buildings. Hence, the shadow fading model can be used to describe the slow fading of the signal.

4.2.1. Simplified multimode model

First, we utilize the GO model [23] to analyze the excitation area. Because the planar air waveguide has dependence on only one coordinate, the excitation plane is degenerated to a line that is perpendicular to the ceiling and floor plane and contains the point of the transmission antenna. The geometry of the cross section is just the same as that of tunnels but with only a y-coordinate. The properties of the images and the reflection rays in the tunnel case are still valid. The difference lies on: (1) only y-coordinate takes effect; and (2) the incident angle on the ceiling and floor is a constant – 0°, hence the reflection reflection coefficient is $(1 - \sqrt{k_h})/(1 + \sqrt{k_h})$ for X-polarized field and $(\sqrt{k_h} - 1)/(\sqrt{k_h} + 1)$ for Y-polarized field. In the following derivation, we assume the transmission antenna is X-polarized. The result for a Y-polarized antenna can be derived in a similar way.

Consider that the transmitter is located at the height y_0, and the observe point is set at the height y. The major field at the observe point is given by:

$$E_x^{Rx} = E_x^{Tx} \cdot \sum_q \left[\frac{\exp(-jky_q(y))}{y_q(y)}\right] \cdot \left(\frac{1-\sqrt{k_h}}{1+\sqrt{k_h}}\right)^{|q|} \quad (34)$$

where, $y_q(y)$ is the distance between image I_q and the receiver, which is given by:

$$y_q(y) = \begin{cases} |2qb - y_0 - y|, & \text{if } q \text{ is odd} \\ |2qb + y_0 - y|, & \text{if } q \text{ is even.} \end{cases} \quad (35)$$

Second, we project the field of excitation line obtained above on the orthogonal eigenfunctions of the planar air waveguide modes, and then derive the mode intensity. The eigenfunctions of X-polarized modes in a planar air waveguide are given by [26]:

$$E_n^x(y) = E_0^x \cdot \cos\left[\left(\frac{n\pi}{2b} - j \cdot \frac{n\pi}{2b^2 k}\frac{k_h}{\sqrt{k_h - 1}}\right) y + \varphi_y\right] \quad (36)$$

where, $\varphi_y = \frac{\pi}{2}$ if n is even; $\varphi_y = 0$ if n is odd.

The mode intensity C_n is derived by projecting the field of excitation area (E_x^{Rx} in (34)) on the basis function E_n^x:

$$\begin{aligned} C_n &= \int_{-b}^{b} E_x^{Rx} \cdot E_n^x(y)\mathrm{d}y \\ &= \sum_q \left[\int_{-b}^{b} E_x^{Tx} \cdot \left[\frac{\exp(-jky_q(y))}{y_q(y)}\right] \right. \\ &\quad \left. \times \left(\frac{1-\sqrt{k_h}}{1+\sqrt{k_h}}\right)^{|q|} \cdot E_n^x(y)\mathrm{d}y\right]. \end{aligned} \quad (37)$$

Use the same numerical integration technique as in the tunnel case, the normalized mode intensity $\overline{C_n}$ is:

$$\begin{aligned} \overline{C_n} \simeq \frac{1}{n}\sqrt{\frac{4a}{3}} \sum_q \left\{\sum_{v=0}^{n-1}\left[\frac{r_0 \exp(-jky_q(y))}{y_q(y) + r_0}\left(\frac{1-\sqrt{k_h}}{1+\sqrt{k_h}}\right)^{|q|}\right.\right. \\ \left.\left. \times (-1)^{\lfloor \frac{n}{2} \rfloor + 1 + v}\right]\right\}. \end{aligned} \quad (38)$$

With the intensity and eigenfunction of each mode, the field at any position can be predicted for the case without pillars.

4.2.2. Shadow fading model and the combined result

The shadow fading model is used to describe the slow fading caused by the reflection and diffraction on those pillars. The amplitude change caused by shadow fading is often modeled using a log-normal distribution [8]. Since one mode can be viewed as a cluster of rays with the same grazing angle, we assume that each mode experiences identically distributed and independent shadow fading when it goes through the pillars. Therefore, the predicted field at any position ($b + y$ m above the floor, z m apart the transmitter) can be obtained by summing up the field of all modes, which is given by:

$$E_x^{Rx}(y,z) = E_0^x \sum_n \overline{C_n} \cdot E_n^x(y) \cdot \frac{1}{2\pi z} \mathrm{e}^{-(\alpha_n + j\beta_n)\cdot z} \cdot \chi_n \quad (39)$$

where $\{\chi_n\}$ are identically distributed and independent log-normal random variables; the field is divided by $2\pi z$ because the plane wave in the room-and-pillar environment spreads in all horizontal directions; α_n is the attenuation coefficient and β_n is the phase-shift coefficient, which is given by [28,26]:

$$\alpha_n = \frac{1}{b}\left(\frac{n\pi}{2bk}\right)^2 \mathrm{Re}\frac{1}{\sqrt{k_h - 1}}; \qquad \beta_n = \sqrt{k^2 - \left(\frac{n\pi}{2b}\right)^2}. \quad (40)$$

The predicted received signal power is given by:

$$\begin{aligned} P_r(y,z) = P_t G_t G_r \left(\frac{1}{2kr_0}\sum_n \overline{C_n} \cdot E_n^x(y) \right. \\ \left. \times \frac{1}{2\pi z}\mathrm{e}^{-(\alpha_n + j\beta_n)\cdot z} \cdot \chi_n\right)^2. \end{aligned} \quad (41)$$

4.3. Comparison with experimental measurements

We validate the multimode model by comparing the theoretical results with the experimental measurements in both tunnel environment and room-and-pillar environment provided in [29,24], respectively.

The experiment in [29] was conducted in a straight road tunnel. The tunnel is 3.5 km long and has an equivalent rectangle (7.8 m wide and 5.3 m high, i.e. $a = 3.9$, $b = 2.65$) cross section shape. In Fig. 9(a), the calculated result at frequencies of 450 MHz and 900 MHz is compared with the measurements shown in [29]. The theoretical curves are vertically displaced by 75 dB and 40 dB, respectively, from the experimental curves for better comparison. It is shown that the curves of the theoretical and experimental results are close to each other. Our multi-mode model accurately predicts the attenuation velocity, the fast fading in the near region, the flat fading in the far region and the effects of different operating frequencies in the tunnel environment.

In [24], the experiment was conducted in a room-and-pillar mining area with an average height of 6 m. In Fig. 9(b), the calculated result at a frequency of 900 MHz is compared with the measurements shown in [24]. It indicates that the theoretical result also has a good agreement with the experimental measurement in the room-and-pillar environment.

4.4. Channel characteristics of road tunnels and underground mines

In this section, we first implement the Multimode model to analyze the channel characteristics under various tunnel conditions. Then we extend our analysis to the room-and-pillar case.

4.4.1. Tunnel channel characteristics

Operating Frequency: Fig. 10 illustrates the effects of operating frequency on the channel characteristics. In particular, in Fig. 10(a) and (b), the signal power and the corresponding power distribution among significant modes are shown as a function of axial distance at frequencies of 500 MHz and 1.5 GHz, respectively. In the near region, the received power attenuates fast and fluctuates very rapidly. This is attributed to the combined effect of multiple modes. On the other hand, in the far region, the decrease in the received power is gradual. This is due to the fact that the higher order modes

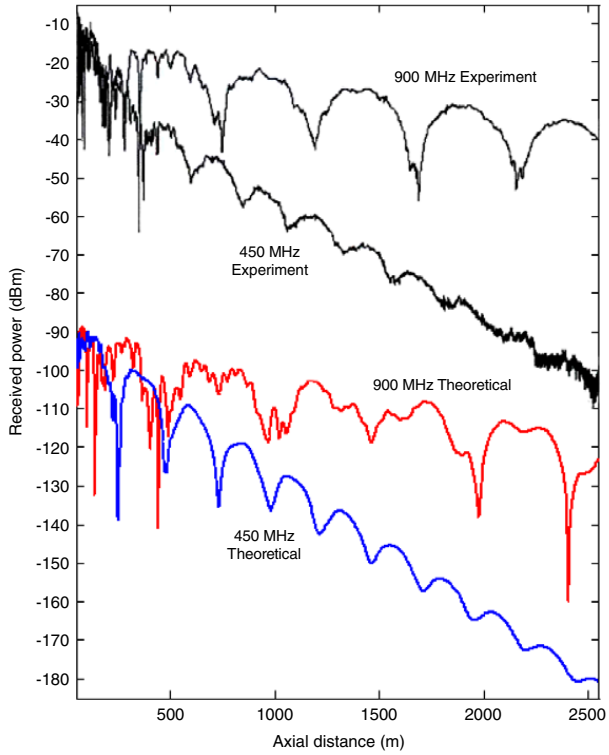

(a) 450 MHz and 900 MHz in a road tunnel (the theoretical result is displaced by 75 dB).

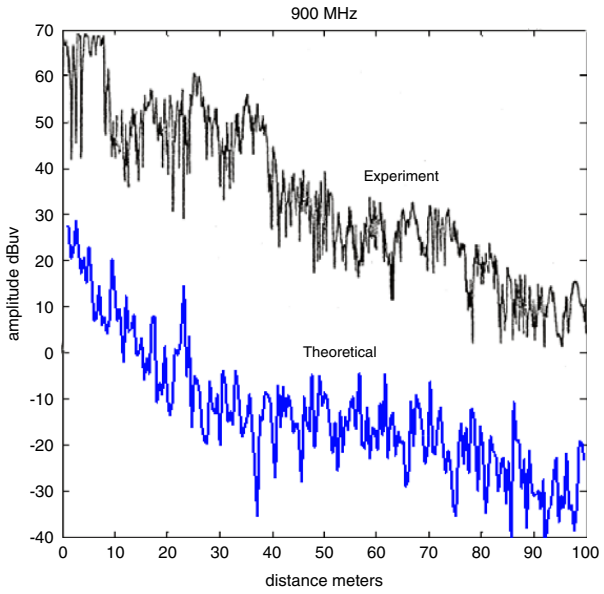

(b) 900 MHz in a room-and-pillar mining area (the theoretical one is displaced by 40 dB).

Fig. 9. Experimental and theoretical received power.

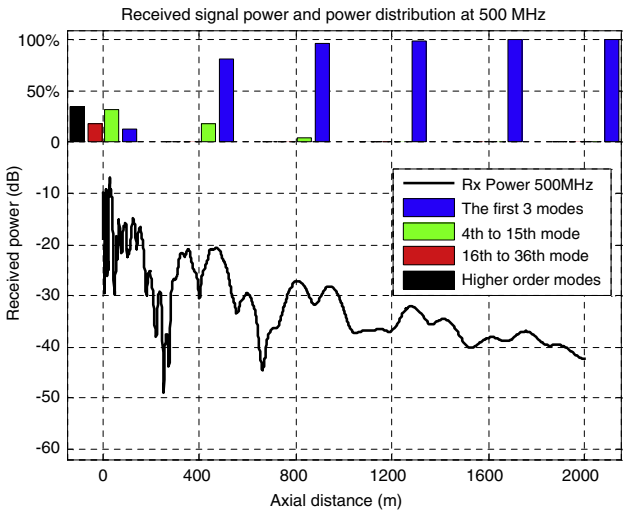

(a) Received signal power and the power distribution among modes at 500 MHz.

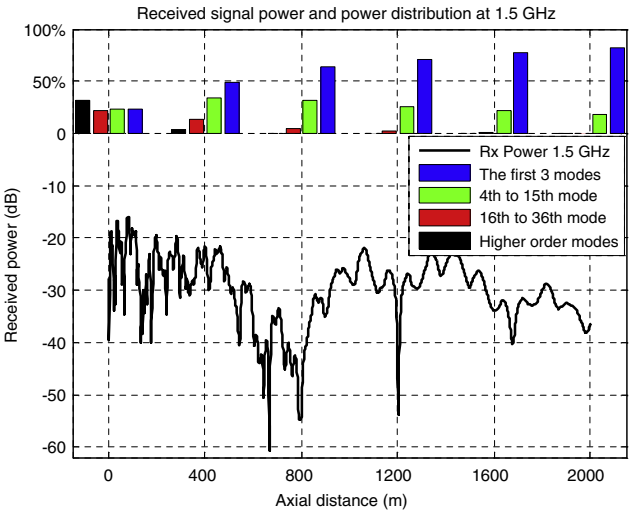

(b) Received signal power and the power distribution among modes at 1.5 GHz.

Fig. 10. Channel characteristics in tunnels at different operating frequencies.

attenuate rapidly as the distance increases. Hence, the field in the far region is governed by the few remaining low-order modes. Although the operating frequency does not affect the power distribution of modes significantly, it has an obvious influence on the propagation constants. Signals with higher frequency attenuate slower. Hence, as frequency increases, the signal attenuation decreases and the length of the fast fluctuating region is increased.

Tunnel size and antenna polarization: The tunnel size has similar effects on the channel characteristics as the operating frequency. In tunnels with larger dimensions, the attenuation constant α_{mn} is smaller and a greater number of modes remain significant in the far region. Therefore, the fast fluctuating region is prolonged in larger tunnels, and vice versa. For horizontal polarized antennas, the tunnel width plays a more important role because the reflection coefficients on the horizontal walls is larger than those on the vertical walls. Hence, the signal attenuates slower and fluctuates longer in larger and wider tunnels for horizontal polarized antenna. Meanwhile, in larger and

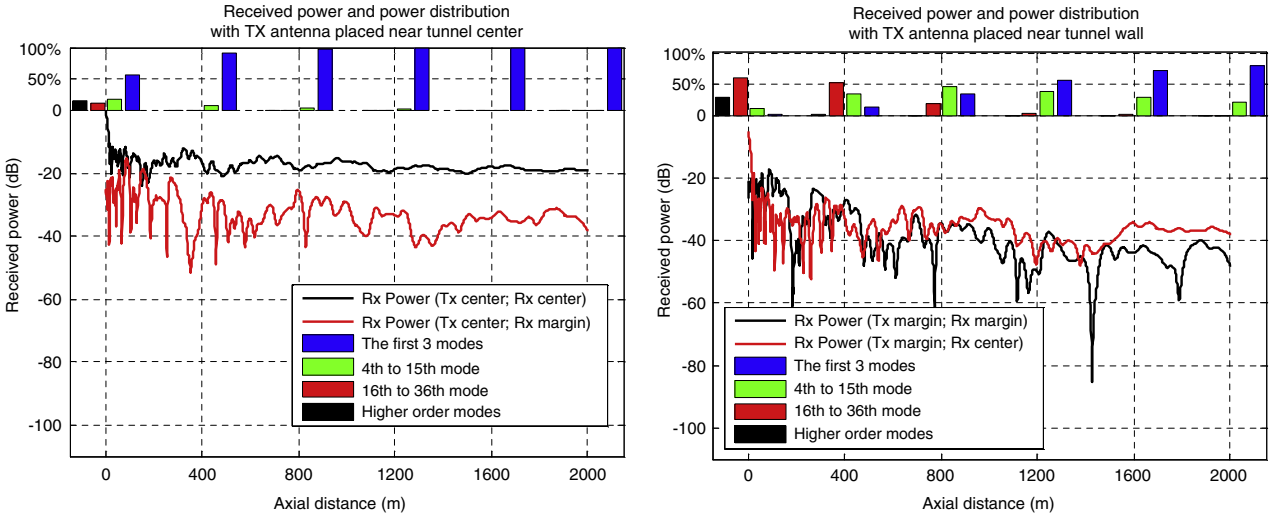

(a) Received signal power and the power distribution among modes when the Tx antenna is placed near the tunnel center.

(b) Received signal power and the power distribution among modes when the Tx antenna is placed near the tunnel wall.

Fig. 11. Channel characteristics with different antenna position and polarization.

higher tunnels, the power of all the modes drops down more slowly for a vertical polarized antenna.

Antenna position: Fig. 11 shows the received power and the power distribution among modes with different antenna positions. The case where the transmitter antenna is placed near the center of the tunnel cross section is shown in Fig. 11(a). The receiver antenna is placed either at the center or at one-eighth of the tunnel height and one-eighth of the tunnel width. It is shown that the lowest modes are effectively excited (over 50% of the total power). If the receiver is also at the center, both the signal attenuation and the fluctuation are small. If the receiver is placed near the tunnel walls, the attenuation and fluctuation are much more significant. In Fig. 11(b), the case where the transmitter antenna is placed near the tunnel wall (1/8 of the width and 1/8 of the height) is shown. The receiver antenna is also placed either at the center or at the border of the tunnel. Near the excitation plane, higher order modes dominate (over 80% of the total power). In this case, the position of the receiver antenna does not affect the received signal. The attenuation and the fluctuation of the received power are significant.

Electrical parameters: The electrical parameters consist of permittivity ε and conductivity σ. The temperature, humidity and pressure have little influence on the air permittivity but may affect the conductivity more. However, the effect of changes in the conductivity of tunnel air may be neglected, because it is very small compared to the permittivity. Therefore, the electrical parameters of tunnel air can be considered the same as those of normal air. The electrical parameters of the tunnel walls are provided in [28], where the permittivity of tunnel materials is in the range of $5\varepsilon_0 \sim 10\varepsilon_0$ (ε_0 is the permittivity in a vacuum) and the conductivity is of the order of 10^{-2} S/m at the UHF frequency band. In this value range, the electrical parameters of either tunnel wall or tunnel air do not influence the signal propagation inside the tunnel considerably.

4.4.2. Room & pillar channel characteristics

The operating frequency, room height, antenna position/polarization, and electrical parameters in the room-and-pillar environment affect signal propagation in a similar way as in the tunnel case. However, their influence is much smaller. Compared to the tunnel case, signals in a room-and-pillar mining area experience extra multipath fading caused by the pillars. Consequently, a higher path loss is experienced by the waves spreading in the room.

5. Challenges in the design of WUCNs

Analysis of the signal propagation techniques in both the soil medium and the underground mines/tunnels highlights the peculiarities of the transmission media. Consequently, the following challenges emerge in the design of WUCNs.

5.1. WUCNs in soil medium using EM waves

5.1.1. Topology design

The results for the maximum attainable communication range in Section 2 illustrates that an underground environment is much more limited compared to terrestrial WSNs. Consequently, in the design of WUCN topology, multi-hop communication should be emphasized.

Another important factor is the direct influence of soil properties on the communication performance. It is clear that any increase in water content significantly hampers communication quality. The network topology should be designed to be robust to such changes in channel conditions. Furthermore, soil composition at a particular location should be carefully investigated to tailor the topology design according to specific characteristics of the underground channel at that location.

Moreover, the underground communication is also affected by the changes according to depth. As a result, different ranges of communication distance can be attained at different depths. This requires a topology structure that is

adaptive to the 3D effects of the channel. Optimum strategies to provide connectivity and coverage should be developed considering these peculiarities.

5.1.2. Operating frequency

Our channel model clearly illustrates the fact that the attenuation increases with operating frequency, which motivates smaller frequency values considering the high attenuation. However, this results in a trade off between the frequency and the antenna size.

Additionally, the communication performance at low depth reveals that using a fixed operating frequency may not be the best option for WUCNs. Furthermore, our analysis reveals that the optimal frequency to reach the maximum communication range varies by depth. Consequently, cognitive radio techniques [30] can provide an adaptive operation for the WUCNs in this dynamic environment.

5.1.3. Cross-layer and environment-aware protocol design

Our channel model reveals that the communication quality is also related to the environmental conditions. Besides the effect of soil type, seasonal changes result in a variation of volumetric water content, which significantly affects the communication performance. Therefore, in the protocol design for WUCNs, the environment dynamics need to be considered. This implies an *environment-aware protocol* that can adjust the operation parameters according to the surroundings. Furthermore, the dynamic nature of the physical layer and its direct influence on communication quality call for novel cross layer design techniques that are adaptive to environmental changes for WUCNs. We provide an initial step based on this concept through a packet size optimization framework for WUCNs in [31].

5.2. WUCNs in soil medium using MI waveguide

5.2.1. Topology design

Compared with the EM wave techniques, the MI waveguide technique addresses the challenges of the dynamic channel condition and the large antenna size. Additionally, it reduces the path loss by 50%. However, the transmission range (around 10 m) is still limited. Hence, multi-hop communication is still essential in the MI waveguide case. Moreover, multiple relay coils need to be deployed between the transceivers. Even though the relay coils do not consume energy and the cost is very low, the deployment of these coils requires significant labor. Hence, the network topology of the WUCNs needs to be carefully designed.

5.2.2. Generalization of the channel model for multi-hop communication in 3D networks topology

The MI waveguide provided in Section 3 is limited to the one-dimensional (1D) planar structure. Moreover, the communication is limited to the point-to-point case. However, in the WUCNs, the network topology is three-dimensional (3D). The MI waveguide structure is no longer a simple line but may become a more complicated 3D structure. Furthermore, the relay coils in different links may influence each other in the 3D space. Hence, a channel model for multi-hop communication in 3D networks needs to be developed.

5.2.3. Adaptive operating frequency assignment and error control

Although soil properties do not affect the communication using an MI waveguide, other environment factors may still influence the channel. First, the position of the relay coils may change while the network is operating due to the above ground pressure or movement of the soil. Second, the capacitor value of the relay coil may drift due to a change of humidity or temperature. Since the operating frequency is precisely designed according to those parameters to achieve the low path loss, a fixed operating frequency cannot guarantee the optimum system performance if the parameters change. Hence, the cognitive radio techniques [30] can provide an adaptive operation for the MI waveguide. Moreover, if the positions or the capacitor values of the relay coils change significantly, the path loss of the MI waveguide may dramatically increase even if cognitive radio techniques are adopted. Consequently, schemes of adaptive error control need to be developed for WUCNs using an MI waveguide.

5.3. WUCNs in underground mines and road/subway tunnels

5.3.1. Reliability

The channel characteristics results illustrate that the radio signal experiences deep fading at different positions in the tunnels, which causes *dead zones*. The position of the dead zones is determined by the operating frequency, the tunnel size, the position and the polarization of the transmitting antenna. Since the reliability is the most essential requirement for communications in underground mines and tunnels, physical layer techniques, such as MIMO and adaptive OFDM, need to be analyzed to cover the dead zones.

5.3.2. Network architecture design

The structures of the underground mines are analyzed in Section 4. The network architecture of WUCNs is significantly different from the terrestrial case and need to be analyzed, since all the transceivers are confined in the labyrinth of the mine and radio links only exist along the tunnels. Moreover, the human activity in underground mines can be modeled to provide more information for the network architecture design.

5.3.3. Localization techniques

The position information is very important in underground mines and road/subway tunnels for both communication networks and sensor networks. However, GPS devices do not work and the signal propagation has different characteristics in underground mines and tunnels. Hence, new localization algorithms and distance measurements techniques specifically for underground environments need to be developed.

5.3.4. Mobility support

The WUCNs are constructed for communication among human beings and vehicles in underground mines and tunnels. The communication should not be interrupted when these network nodes are moving. Since the environments have unique channel characteristics, the influence of mobility on the communication is different from the terrestrial case. Hence physical layer techniques and communication protocols should be developed to support the node mobility in such specific underground environments.

5.3.5. Cross-layer protocol design

As indicated in our channel model in Section 4, the communication quality is related to multiple environment parameters, such as tunnel size and antenna position/polarization. Therefore, in the protocol design for WUCNs, those parameters need to be considered. Cross-layer communication protocol may recognize the environment parameters and adaptively change the operating parameters to achieve the optimum system performance.

6. Conclusion

In this paper, an overview of underground wireless channel models and corresponding challenges are provided for Wireless Underground Communication Networks (WUCNs). More specifically, the WUCNs are classified into two major classes based on the environment they operate in: soil medium and underground mines/tunnels.

For WUCNs in soil medium, channel models for EM and MI waves are described. First, a complete underground channel model is derived to characterize the EM wave propagation. Analysis shows that communication success significantly depends on the operating frequency and the composition of the soil. Furthermore, it is shown that the channel characteristics depend on the burial depth of the sensors. For low depth deployments, the channel is shown to exhibit a two-path channel, while for high depth deployments, a single path channel is suitable to characterize communication. Besides EM waves, an MI waveguide is developed as an alternative wireless communication technique in a soil medium. Although a traditional MI technique addresses the dynamic channel conditions and large antenna size challenges of EM waves in soil medium, the MI signal attenuates much faster than the EM wave signal. The proposed MI waveguide technique can greatly reduce the path loss through the relay coils deployed between the transceivers.

For WUCNs in underground mines/tunnels, we analyze the typical structures of underground mines and road tunnels. Accordingly, the channel model is investigated for two cases: tunnel and room-and-pillar models. The *multimode model* is presented to completely characterize the EM wave propagation for both cases. In tunnel environments, high signal attenuation and intense fluctuation occur in the near region due to the combination of multiple modes. In the far region, the fall of the received power is gradual because the higher order modes attenuate very fast as the distance increases. The speed of the signal attenuation is mostly determined by the tunnel size and operating frequency, while the energy distribution among modes is governed by the position of the transmitter antenna. Signal propagation in room and pillar environments has similar characteristics as in the tunnel case except the fact that signals experience significant fluctuations in both near and far regions. Additionally, the influence of operating frequency, room height, antenna position/polarization and electrical parameters is much smaller than in the tunnel case.

Wireless underground communication networks (WUCNs) promise extensive capabilities for a wide array of applications that were not possible before. However, the analysis provided in this paper reveal that the communication characteristics in these networks significantly depend on the environment properties and should be analyzed accordingly. The channel models provided for different media in this paper lay out the foundations and highlight challenges for novel communication techniques tailored to the underground communication paradigm. We believe these challenges will stimulate the establishment of new research areas for the realization of WUCNs.

Acknowledgment

This work is based upon work supported by the US National Science Foundation (NSF) under Grant No. CCF-0728889.

References

[1] I.F. Akyildiz, E.P. Stuntebeck, Wireless underground sensor networks: Research challenges, Ad Hoc Networks Journal 4 (2006) 669–686.
[2] M.C. Vuran, I.F. Akyildiz, Channel modeling and analysis for wireless underground sensor networks, 2008 (submitted for publication).
[3] L. Li, M.C. Vuran, I.F. Akyildiz, Characteristics of underground channel for wireless underground sensor networks, in: Proc. IFIP Mediterranean Ad Hoc Networking Workshop (Med-Hoc-Net '07), Corfu, Greece, June 2007.
[4] Z. Sun, I.F. Akyildiz, Magnetic induction waveguide: A new propagation technique for underground wireless communication, 2008 (submitted for publication).
[5] Z. Sun, I.F. Akyildiz, Underground wireless communication using magnetic induction, in: Proc. IEEE ICC 2009, Dresden, Germany, June 2009 (in press).
[6] Z. Sun, I.F. Akyildiz, Channel modeling and analysis for wireless networks in underground mines and road tunnels, 2008 (submitted for publication).
[7] Z. Sun, I.F. Akyildiz, Channel modeling of wireless networks in tunnels, in: Proc. IEEE GLOBECOM 2008, New Orleans, USA, November, 2008.
[8] G. Stuber, Principles of Mobile Communication, Kluwer Academic Publishers, 1996, 2/e 2001.
[9] N. Peplinski, F. Ulaby, M. Dobson, Dielectric properties of soils in the 0.3-1.3-GHz range, IEEE Transactions on Geoscience and Remote Sensing 33 (3) (1995) 803–807.
[10] A.R. Silva, M.C. Vuran, Empirical evaluation of underground-to-underground communication in wireless underground sensor networks, in: Proc. IEEE DCOSS 2009, Marina Del Rey, CA, 2009.
[11] J.R. Holdem, et al., Estimation of the number of frequencies and bandwidth for the surface measurement of soil moisture as a function of depth, IEEE Transactions on Instrumentation and Measurement 49 (5) (2000) 964–970.
[12] H. Li, Z. Dong, L. Wang, Research on temporal and spatial variety of soil moistures of shifting sand dune and four main plant communities on otindag sandy land, Journal of Arid Land Resources and Environment 20 (3) (2006).
[13] K. Zhang, W. Peng, L. Wang, A. Fu, X. Xu, Variation of soil temperature and soil moisture on black soil profile in seasonal frozen area of northeast China, Georgraphical Research 26 (2) (2007).
[14] N. Jack, K. Shenai, Magnetic Induction IC for Wireless Communication in RF-Impenetrable Media, in: IEEE Workshop on Microelectronics and Electron Devices, WMED 2007, April 2007.
[15] J.J. Sojdehei, P.N. Wrathall, D.F. Dinn, Magneto-inductive (MI) communications, MTS/IEEE Conference and Exhibition, OCEANS 2001, 2001.

[16] R. Bansal, Near-field magnetic communication, IEEE Antennas and Propagation Magazine (2004).
[17] C. Bunszel, Magnetic induction: A low-power wireless alternative, RF Design 24 (11) (2001) 78–80.
[18] D.R. Frankl, Electromagnetic Theory, Prentice-Hall, Englewwod Cliffs, NJ, 1986.
[19] R.E. Gertsch, R.L. Bullock, Techniques in underground mining: Selections from Underground mining methods handbook, Littleton, CO: Society for Mining, Metallurgy, and Exploration, 1998.
[20] A.G. Emslie, R.L. Lagace, P.F. Strong, Theory of the propagation of UHF radio waves in coal mine tunnels, IEEE Transactions on Antenna and Propagation AP-23 (2) (1975) 192–205.
[21] Y.P. Zhang, G.X. Zheng, J.H. Sheng, Excitation of UHF radio waves in tunnels, Microwave and Optical Technology Letters 22 (6) (1999) 408–410.
[22] C. Cerasoli, RF propagation in tunnel environments, in: Proceedings of IEEE Military Communications Conference, 2004 - MILCOM 2004, vol. 1, 2004, pp. 363–369.
[23] S.F. Mahmoud, J.R. Wait, Geometrical optical approach for electromagnetic wave propagation in rectangular mine tunnels, Radio Science 9 (12) (1974) 1147–1158.
[24] M. Lienard, P. Degauque, Natural wave propagation in mine environments, IEEE Transactions on Antenna and Propagation 48 (9) (2000) 1326–1339.
[25] K.D. Laakmann, W.H. Steier, Waveguides: Characteristic modes of hollow rectangular dielectric waveguides, Applied Optics 15 (5) (1976) 1334–1340.
[26] D. Porrat, Radio propagation in hallways and streets for UHF communications, Ph.D Thesis, Stanford University, 2002.
[27] J.M. Molina-Garcia-Pardo, M. Lienard, P. Degauque, D.G. Dudley, L. Juan-Llacer, Interpretation of MIMO channel characteristics in rectangular tunnels from modal theory, IEEE Transactions on Vehicular Technology 57 (3) (2008) 1974–1979.
[28] P. Delogne, Leaky Feeders and Subsurface Radio Communications, P. Peregrinus, New York, 1982, Stevenage, Herts.
[29] D.G. Dudley, M. Lienard, S.F. Mahmoud, P. Degauque, Wireless propagation in tunnels, IEEE Antenna and Propagation Magazine 49 (2) (2007) 11–26.
[30] I.F. Akyildiz, W.Y. Lee, M.C. Vuran, S. Mohanty, Next generation/dynamic spectrum access/cognitive radio wireless networks: A survey, Computer Networks Journal 50 (2006) 2127–2159.
[31] M.C. Vuran, I.F. Akyildiz, Packet size optimization for wireless terrestrial, underwater, and underground sensor networks, in: Proc. IEEE INFOCOM '08, Phoeniz, AZ, 2008.

Ian F. Akyildiz received the B.S., M.S., and Ph.D. degrees in Computer Engineering from the University of Erlangen-Nuernberg, Germany, in 1978, 1981 and 1984, respectively.

Currently, he is the Ken Byers Distinguished Chair Professor with the School of Electrical and Computer Engineering, Georgia Institute of Technology, Atlanta, and Director of Broadband Wireless Networking Laboratory. Since June 2008, he is an Honorary Professor with the School of Electrical Engineering at the Universitat Politecnico de Catalunya, Barcelona, Spain. He is the EditorinChief of *Computer Networks (COMNET) Journal (Elsevier)* as well as the founding EditorinChief of the *AD HOC NETWORK JOURNAL (Elsevier)* and *PHYSICAL COMMUNICATION (PHYCOM) JOURNAL (Elsevier)*. His current research interests are in cognitive radio networks, wireless sensor networks, wireless mesh networks, and nanocommunications.

He received the "Don Federico Santa Maria Medal" for his services to the Universidad of Federico Santa Maria, in 1986. From 1989 to 1998, he served as a National Lecturer for ACM and received the ACM Outstanding Distinguished Lecturer Award in 1994. He received the 1997 IEEE Leonard G. Abraham Prize Award (IEEE Communications Society) for his paper entitled "Multimedia Group Synchronization Protocols for Integrated Services Architectures" published in the IEEE JOURNAL OF SELECTED AREAS IN COMMUNICATIONS (JSAC) in January 1996. He received the 2002 IEEE Harry M. Goode Memorial Award (IEEE Computer Society) with the citation "for significant and pioneering contributions to advanced architectures and protocols for wireless and satellite networking". He received the 2003 IEEE Best Tutorial Award (IEEE Communication Society) for his paper entitled "A Survey on Sensor Networks", published in IEEE COMMUNICATIONS MAGAZINE, in August 2002. He also received the 2003 ACM Sigmobile Outstanding Contribution Award with the citation "for pioneering contributions in the area of mobility and resource management for wireless communication networks". He received the 2004 Georgia Tech Faculty Research Author Award for his "outstanding record of publications of papers between 1999-2003". He also received the 2005 Distinguished Faculty Achievement Award from School of ECE, Georgia Tech. He has been a Fellow of the Association for Computing Machinery (ACM) since 1996.

Zhi Sun received his B.S. degree from Department of Communication Engineering, Beijing University of Posts and Telecommunications (BUPT), and M.S. degree from Department of Electronic Engineering, Tsinghua University, Beijing, China in 2004 and 2007, respectively. Currently, he is a graduate research assistant in Broadband Wireless Networking Laboratory (BWN Lab), School of Electrical and Computer Engineering, Georgia Institute of Technology, Atlanta, GA. He is pursuing Ph.D. degree under the supervision of Prof. Ian F. Akyildiz. His current research interests are in Wireless Underground Communication Networks and Wireless Sensor Networks.

Mehmet C. Vuran received his B.Sc. degree in Electrical and Electronics Engineering from Bilkent University, Ankara, Turkey, in 2002. He received his M.S. and Ph. D. degrees in Electrical and Computer Engineering from the Broadband and Wireless Networking Laboratory, School of Electrical and Computer Engineering, Georgia Institute of Technology, Atlanta, in 2004 and 2007, respectively, under the guidance of Prof. Ian F. Akyildiz.

Currently, he is an Assistant Professor in the Department of Computer Science and Engineering at the University of Nebraska-Lincoln. Dr. Vuran received the 2007 ECE Graduate Research Assistant Excellence Award from School of Electrical and Computer Engineering, Georgia Institute of Technology and the 2006 Researcher of the Year Award in Broadband and Wireless Networking Laboratory, School of Electrical and Computer Engineering, Georgia Institute of Technology. He serves as an Associate Editor of Computer Networks (Elsevier) and Journal of Sensors (Hindawi) journals. He is the guest editor of ACM Monet Journal special issue on Wireless Heterogeneous Networks and Next Generation Internet and Computer Communications Journal special issue on Cognitive Radio and Dynamic Spectrum Sharing Systems. His current research interests include cross-layer design and correlation-based communication for wireless sensor networks, underground sensor networks, cognitive radio networks, and deep space communication networks.